Chapter

Numerical Investigation of Natural Convection and Entropy Generation of Water near Density Inversion in a Cavity Having Circular and Elliptical Body

Nguyen Minh Phu and Nguyen Van Hap

Abstract

In this chapter, a water-filled square cavity with left hot wall and right cold wall was numerically investigated. The hot and cold wall temperatures are 10°C and 0°C respectively to examine the density inversion of natural convection water, i.e. water at 4°C. In the middle of the square, there are circular and elliptical bodies to study fluid–structure interaction in terms of the thermohydraulic behavior and entropy generation. 2D numerical simulation was performed using finite volume method in Ansys fluent software with the assumption of laminar flow. The simulation results are compared with benchmark data to determine reliability. The results indicate that the body insertions increase the convection heat transfer coefficients at the best heat transfer positions due to impingement heat transfer. An increase in heat transfer rate of 1.06 times is observed in the case of circular body compared to none. There are three primary eddies in the cavity with bodies, whereas the cavity without body has two primary eddies. Maximum entropy generation was found in the upper right corner of cavity mainly due to high horizontal temperature gradient. Bodies of circle and vertical ellipse have almost the same thermohydraulic and entropy generation characteristics due to the same horizontal dimension which mainly effects on the downward natural convection current. The entropy generation of cavity with circular body is 1.23 times higher than that of the cavity without body. At positions y/L = 1 on the hot wall and y/L = 0.74 on the cold wall, the convection heat transfer coefficient is close to zero due to stagnant fluid.

Keywords: natural convection, density inversion, numerical simulation, entropy generation, fluid-conic structure interaction

1. Introduction

Water is a fluid with special thermophysical properties compared to many pure substances. That is, the specific heat of water is so large that water is often thought of as a thermal storage media and the density inversion around 4°C alters the natural convection heat transfer mechanism around this temperature [1]. Early, Sasaguchi et al. [2, 3] examined water cooling with density inversion

taken into account. They concluded that the position in vertical direction of the cold cylinder surface had a remarkable effect on the rate of water cooling. Tong [4] reported the effect of the aspect ratio of the cavity on the natural convection heat transfer rate of water around its maximum density. The results show that the aspect ratio of 3 enhances the density inversion. Varol et al. [5] investigated a rectangular cavity with porous media. Flow pattern and isotherms have been presented and analyzed in this study at different Rayleigh numbers. Recently, Hu et al. [6] numerically investigated circular, rectangular, and triangular cavity with inner blocks of circles, squares and triangles. They concluded that increasing the aspect ratio increases the number of vortex and that the effect of cavity's shape on heat transfer is stronger than that of the inner blocks. More recently, Cho et al. [7] simulated natural convection in a cavity with circular and elliptical objects. They confirmed that the elliptical object placed at top increased the Nusselt number by 2.1% compared to the two circular objects [8].

The above works have been done regarding the thermo-hydraulic properties of natural convection in an enclosure. Entropy generation or exergy destruction is a second consideration to comprehensively evaluate an energy system to fulfill the laws of thermodynamics [9–11]. However, the entropy generation assessment due to natural convection in an enclosure with internal objects has been little interest by researchers. Some of the works that can be found in literature are as follows. Kashani et al. [12] investigated entropy generation due to natural convection in an enclosure with vertical wavy walls. They reported that both thermal hydraulics phenomena and entropy generation are strongly influenced by density inversion. Tayebi and Chamkha [13] investigated the entropy generation of a nanofluid in a square cavity with a conducting empty cylinder. Results showed that inserting the cylinder significantly changed the heat transfer mechanism and the irreversibility of the enclosure. Li et al. [14] examines a cylinder inside an inclined enclosure. The effects of radiation and electromagnetic fields on natural convection and entropy production were considered in this study. They reported that the largest Bejan number was reached at an inclination angle of 60°.

From the literature review above, it can be seen clearly that the addition of objects into the cavity alters the thermal properties, fluid flow and entropy generation in natural convection. However, a study of natural convection of water around its maximum density with circular and elliptical objects within cavity has not been found. In this chapter, both the thermohydraulic and entropy generation mechanisms of the above problem were investigated to characterize the energy and exergy aspects of the density inversion associated with the inserts.

2. Model description and validation

Figure 1 shows the 38 mm square cavity examined in this study. Inside the cavity there are circular and elliptical bodies with basic dimensions of 18 mm and 9 mm. The cavity without body is considered as base case (Case 1). The five different conic sections of the body include circle (Case 2), vertical ellipse (Case 3), horizontal ellipse (Case 4), left inclined ellipse (Case 5), and right inclined ellipse (Case 6). Accelerate gravity vector is vertical and in the opposite direction to the y-axis to investigate natural convection in the cavity. The boundary conditions of the computational domain include the temperature T_H = 10°C in the left wall, T_C = 0°C in the right wall. The remaining walls are considered adiabatic. Natural convection currents in cavity are assumed laminar, two-dimensional and incompressible fluid [2, 3, 6, 15]. The following equations are the governing equations under current consideration:

Continuity equation

$$\frac{\partial u}{\partial x}+\frac{\partial v}{\partial y}=0 \tag{1}$$

x-momentum

$$u\frac{\partial u}{\partial x}+v\frac{\partial u}{\partial y}=-\frac{1}{\rho_0}\frac{\partial p}{\partial x}+\frac{\mu}{\rho_0}\left(\frac{\partial^2 u}{\partial x^2}+\frac{\partial^2 u}{\partial y^2}\right) \tag{2}$$

y-momentum

$$u\frac{\partial v}{\partial x}+v\frac{\partial v}{\partial y}=-\frac{1}{\rho_0}\frac{\partial p}{\partial y}+\frac{\mu}{\rho_0}\left(\frac{\partial^2 v}{\partial x^2}+\frac{\partial^2 v}{\partial y^2}\right)-g(\rho-\rho_0) \tag{3}$$

Energy equation

$$u\frac{\partial T}{\partial x}+v\frac{\partial T}{\partial y}=\frac{k}{c_p\rho_0}\left(\frac{\partial^2 T}{\partial x^2}+\frac{\partial^2 T}{\partial y^2}\right) \tag{4}$$

where ρ_0 is the reference density of water, its value of 999.8 kg/m^3 in the present study.

The density of water in the temperature range from 0 to 10°C was fitted from the EES software (F-chart software) as follows:

$$\rho=-7218.26287+106.273748T-0.517050664T^2+0.0011246302T^3 -9.25648144\times10^{-7}T^4 \tag{5}$$

where ρ is water density (kg/m^3) and T is water temperature (K).

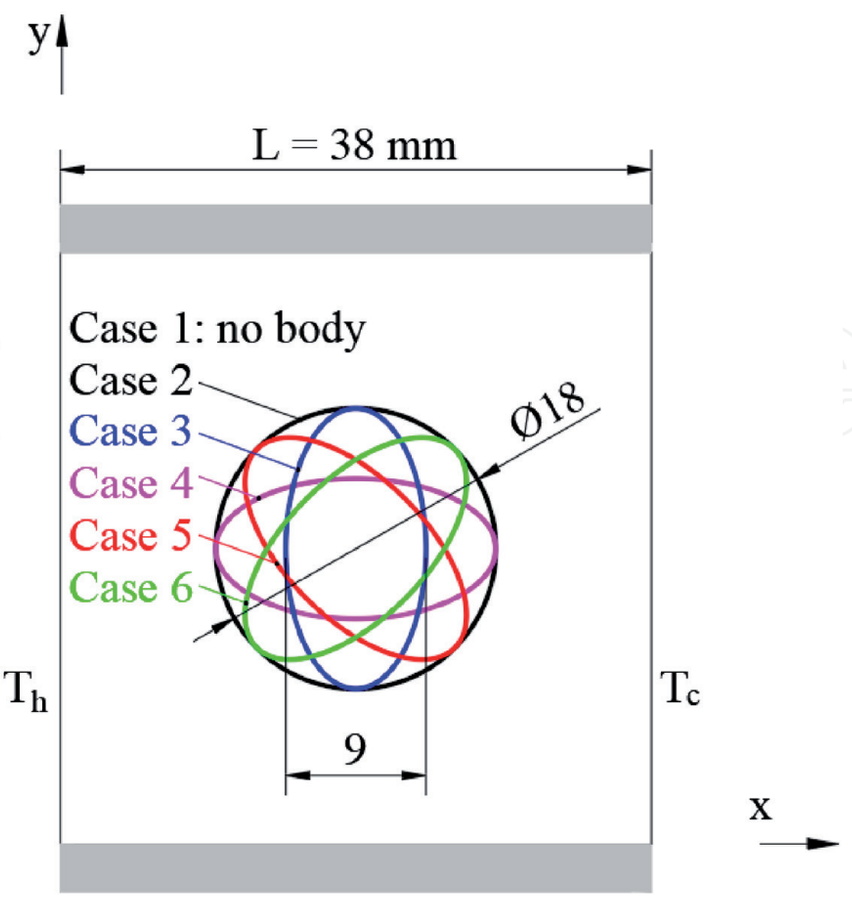

Figure 1.
Computational domain and investigated cases.

It can be observed the difficulty when dealing with the Navier–Stokes governing equation. This is due to the fact that left hand side of the momentum equations is non-linear term. Secondly, a pressure variable does not present in the continuity equation. To overcome drawbacks, a semi-implicit method was adopted in the present numerical study. The selected method is SIMPLE (Semi-Implicit Method for Pressure Linked Equations) algorithm which linearizes convection term in momentum equations and is used to couple velocity and pressure variables in Eqs. (1) and (2). Application of the SIMPLE algorithm to curved surfaces of circle and ellipse can be resolved by an interpolation between grid vertexes which are not coincident with the boundaries leading to low accuracy of the solution. Therefore, the geometric imperfection is eliminated by using a curvilinear coordinate system [16, 17].

Figure 2 shows the meshing in a typical computational domain. Refinements are enhanced for the surfaces to increase accuracy in predicting phenomena in conjunction with the boundary layer. For hybrid grids as displayed in **Figure 2** and enlarged in **Figure 3a**, the velocity and pressure variables are stored in the center of a control volume as illustrated in **Figure 3b**. Thus, these qualities at a face could be interpolated by center-stored pressure and velocity of two adjacent control volumes. The face interpolation can be treated by using the curvilinear coordinate system ξ-η as seen in **Figure 3c** where **n** is the vector normal to the face, $\mathbf{e}_\xi$ and $\mathbf{e}_\eta$ the unit vectors along ξ-η axes [18].

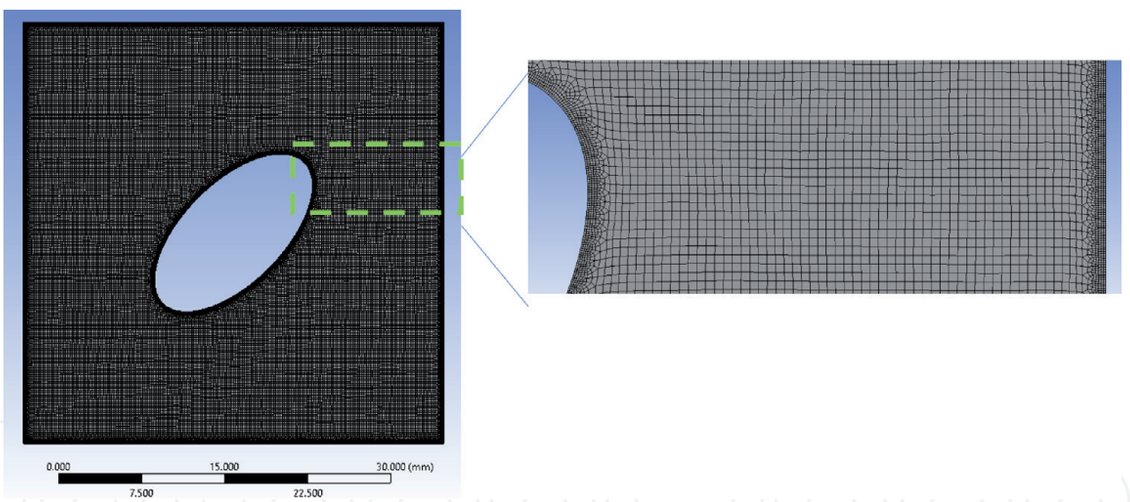

Figure 2.
Mesh generation with refinement.

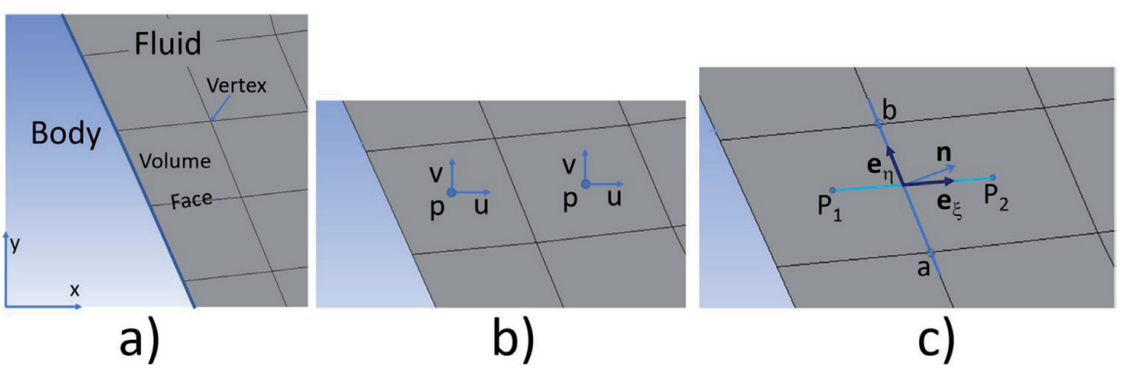

Figure 3.
Face interpolation in finite volume method. (a) Vertex, face, and volume definition. (b) Pressure and velocity components stored in center of a volume. (c) Face interpolation by means of curvilinear coordinate system ξ-η.

Grid independence check for case 1 was conducted with the number of nodes of 18,214, 28,454, 54,609 and 181,524 showing that the number of nodes 54,609 has small error compared with data in the literature and computation cost is moderate. The residuals of 1e-4 and 1e-6 are set for the momentum and energy equations, respectively. **Figure 4** displayed a comparison of velocity components in case 1 along the x-axis at the horizontal center line y = 19 mm with the number of nodes of 54,609, where X = x/L, X-velocity = uL/α, Y-velocity = vL/α, α is the thermal diffusivity. The comparison result with published data [19] showed a fairly good agreement. From these settings and confirmations, grids of about 56,000 nodes are obtained for 5 cases having a body in the middle of cavity.

The thermal and entropy generation parameters were deduced from the simulated data. The local heat transfer coefficient (HTC) at hot and cold walls is computed as:

$$h = \frac{-k\dfrac{\partial T}{\partial x}}{T_H - T_C} \tag{6}$$

where k is the conductivity of water.

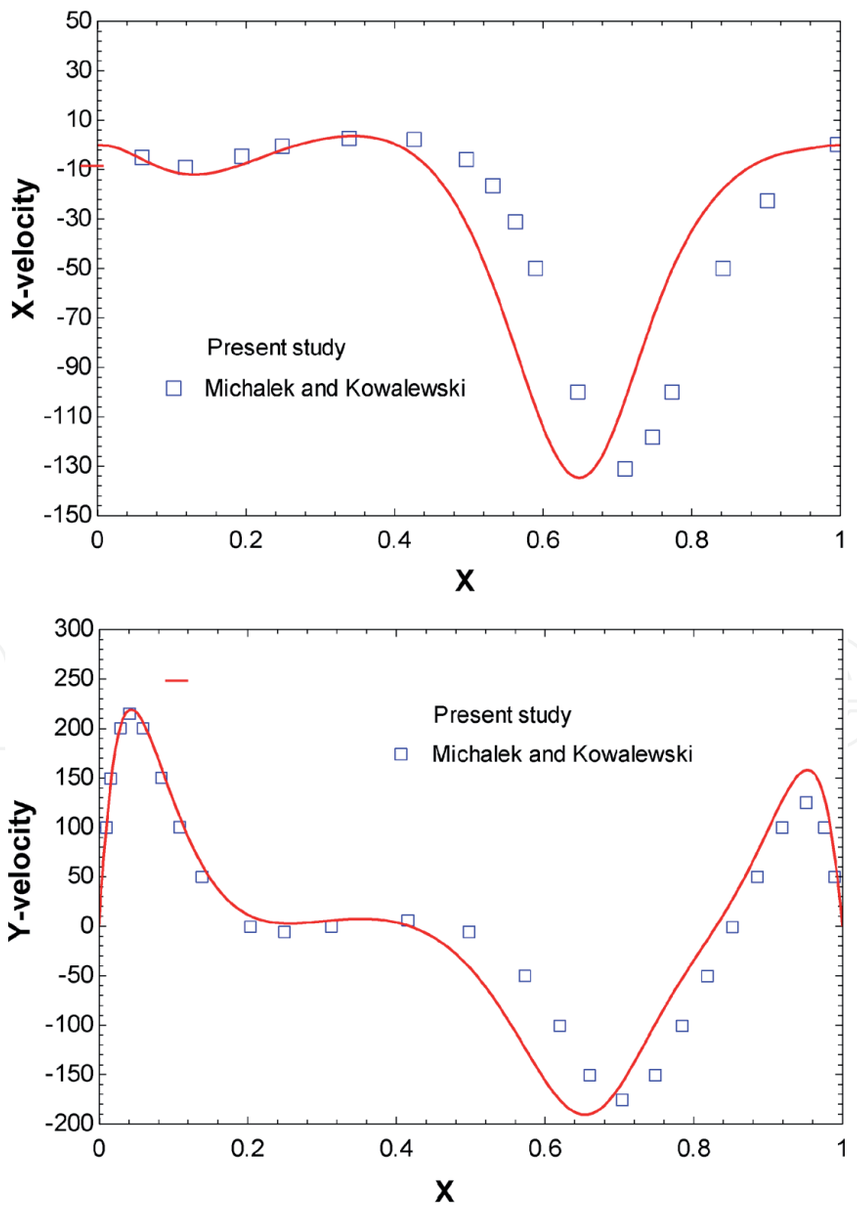

Figure 4.
Validation with published data [19].

The local entropy generation inside the domain can be estimated by [20, 21]:
The local entropy generation due to heat transfer:

$$\dot{S}_t''' = \frac{k}{T^2}\left[\left(\frac{\partial T}{\partial x}\right)^2 + \left(\frac{\partial T}{\partial y}\right)^2\right] \tag{7}$$

The local entropy generation due to fluid friction:

$$\dot{S}_v''' = \frac{\mu}{T}\left\{2\left[\left(\frac{\partial u}{\partial x}\right)^2 + \left(\frac{\partial v}{\partial y}\right)^2\right] + \left(\frac{\partial u}{\partial y} + \frac{\partial v}{\partial x}\right)^2\right\} \tag{8}$$

where μ is the water dynamic viscosity.
Average total entropy generation can be found by the volumetric integral as:

$$\overline{\dot{S}}''' = \frac{1}{V}\int_V \left(\dot{S}_t''' + \dot{S}_v'''\right) dV \tag{9}$$

where V is the volume of computational domain.

3. Results and discussion

Figure 5 shows the velocity distribution in square cavity. Fluid–structure interactions can be clearly observed for six cases. The contour in the **Figure 5** exhibited high-speed upward flow near the heat exchange surfaces and downflow in the middle due to the density difference. The maximum natural convection velocity is about 0.9 mm/s. Case 1 (without body) showed a lightly higher velocity than others due to motion obstruction of the body. It can be seen that the flow pattern of case 2 (circle) and case 4 (horizontal ellipse) is nearly the same. This is because the horizontal size of the two bodies is the same (18 mm). This is the main length that affects downward stream.

The temperature field inside the cavity can be seen in **Figure 6**. The temperature stratifications are clearly visible in the upper half cavity. The upper left corner has

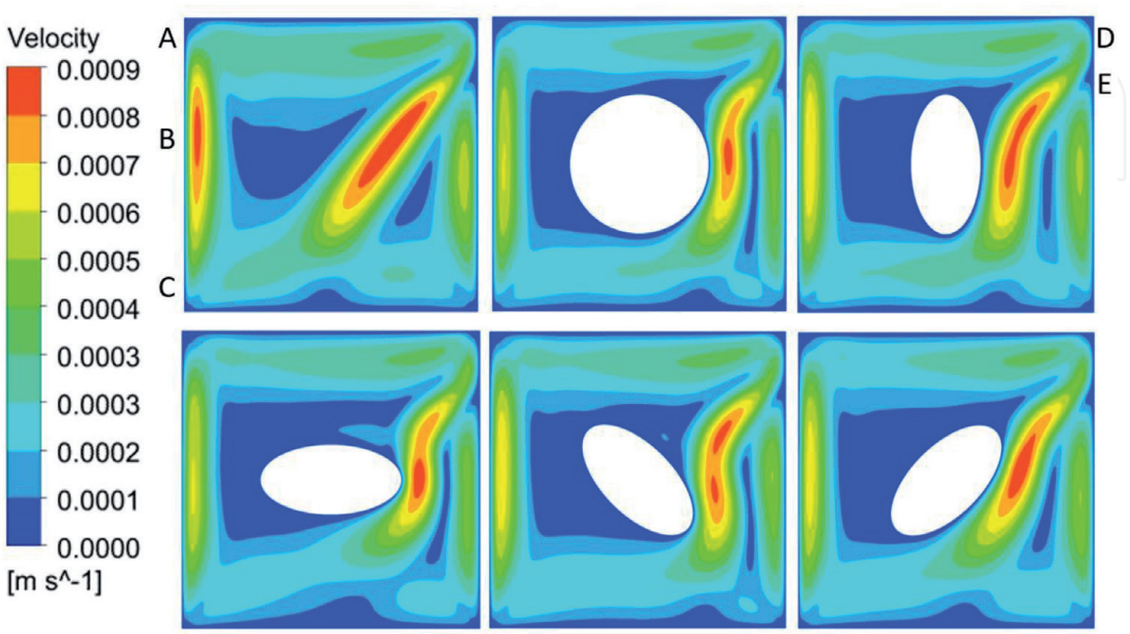

Figure 5.
Velocity magnitude.

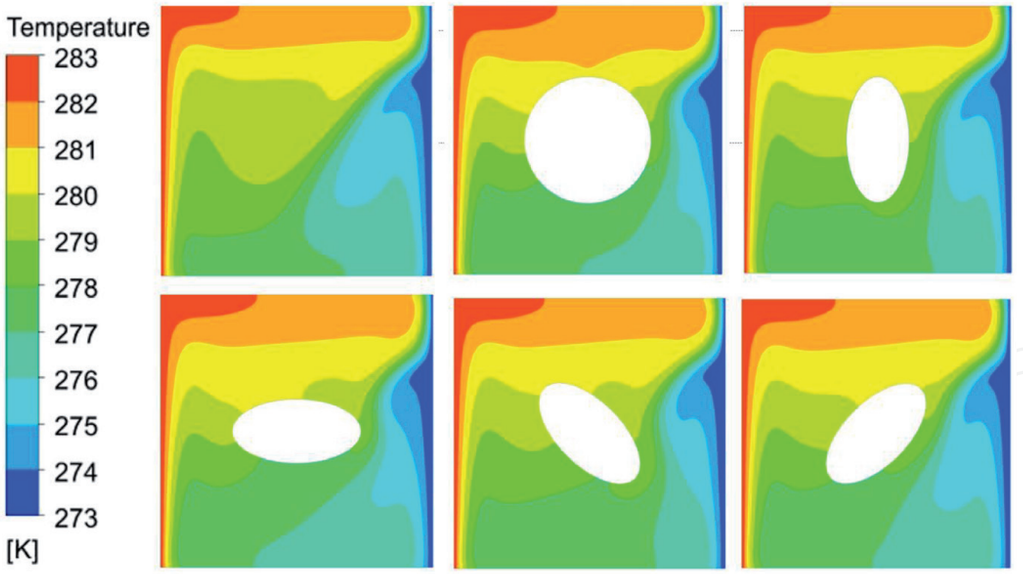

Figure 6.
Isotherms.

high temperature due to the fluid that receives heat from the hot surface and rises. There is a region with relatively low temperature near the cold surface due to the interference between the downstream and the upstream causing stagnant fluid (point E on **Figure 5**).

The flow pattern in the cavity can be observed through the streamlines as shown in **Figure 7**. It is clear that the number of vortices increases from 2 to 3 for the absence of body to its existence. The third swirl located on the upper right side of the body. The one more vortex is formed by the separation of the downstream flow by the bodies. The eddies in the body-inserted cases are smaller than those of the base case due to the occupation of the bodies.

Figure 8 shows the total entropy generation distribution. It can be seen that the largest entropy generation is the upper right corner, the second largest is the lower left corner. Case 2 had the largest entropy generation and case 1 indicated the smallest

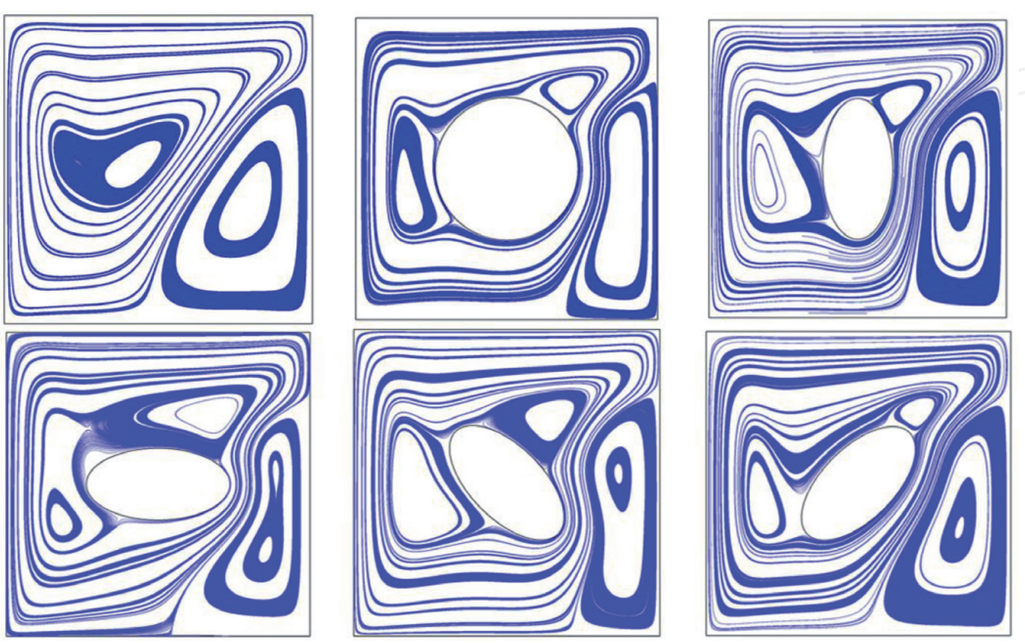

Figure 7.
Streamlines.

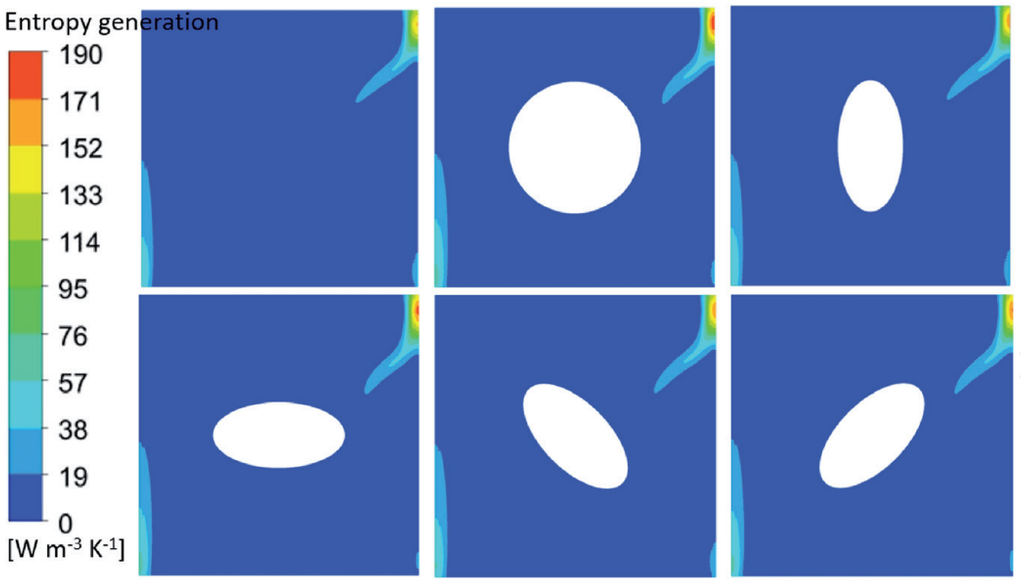

Figure 8.
Total entropy generation.

one. The maximum entropy generation is about 190 W/m^3-K. The entropy generation distribution is quite similar to that of Kashani et al. [12]. The laminar flow and the low velocity lead to small entropy generation due to friction. Entropy generation in the cavity is prevailed by heat transfer. **Figure 9** shows the temperature gradients in case 2 to clarify the effect of the components. Combining **Figures 6** and **9** shows that the horizontal temperature variation is large in the upper right corner. Since downward flow is accompanied by strong heat exchange, the temperature gradient in x direction has considerably high magnitude. The second largest entropy generation is close to the stagnant point on cold wall caused by a large temperature gradient in y-direction. **Figure 10** compares the mean entropy generation for the cases under consideration. The largest and smallest average entropy generations are 3.7 W/ m^3-K and 3 W/m^3-K respectively, corresponding to the entropy generation in case 2 of 1.23 times higher than the base case. The other cases have the average entropy generation of 3.35 W/m^3-K.

Figure 11 reported the local heat transfer coefficient (HTC) on hot and cold surfaces. The largest HTC for the hot surface finds near the bottom wall due to reverse flow causing impingement heat transfer. The local heat transfer coefficient decreased

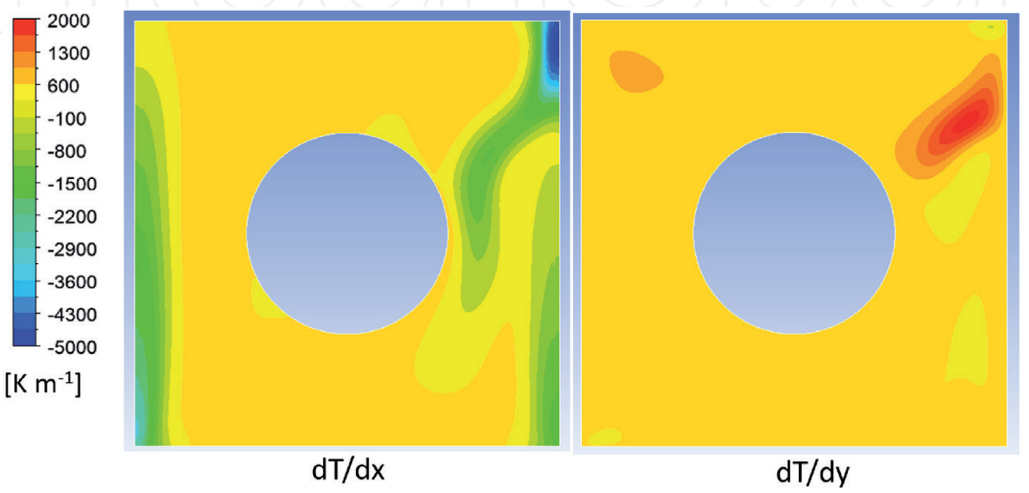

Figure 9.
Temperature gradients in case 2.

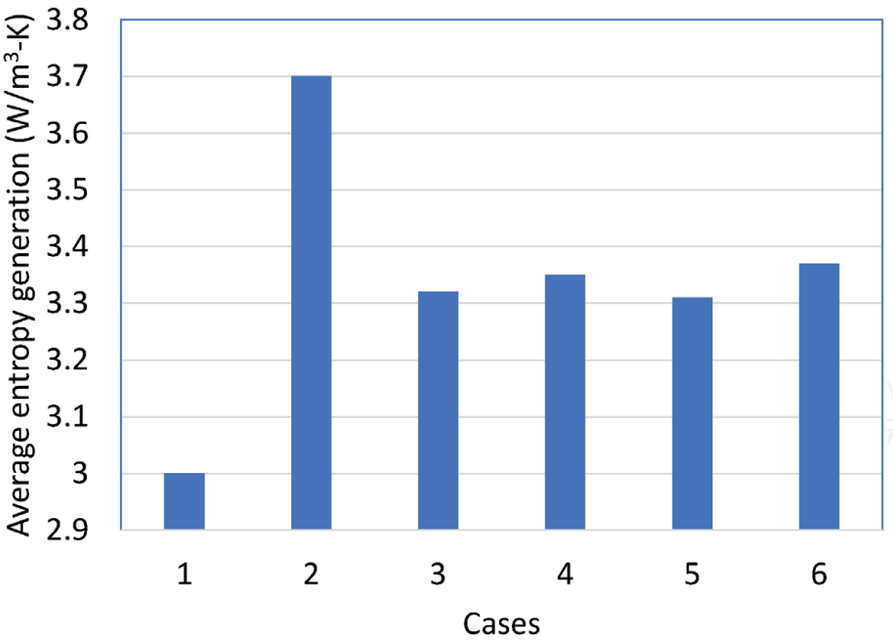

Figure 10.
Average entropy generation.

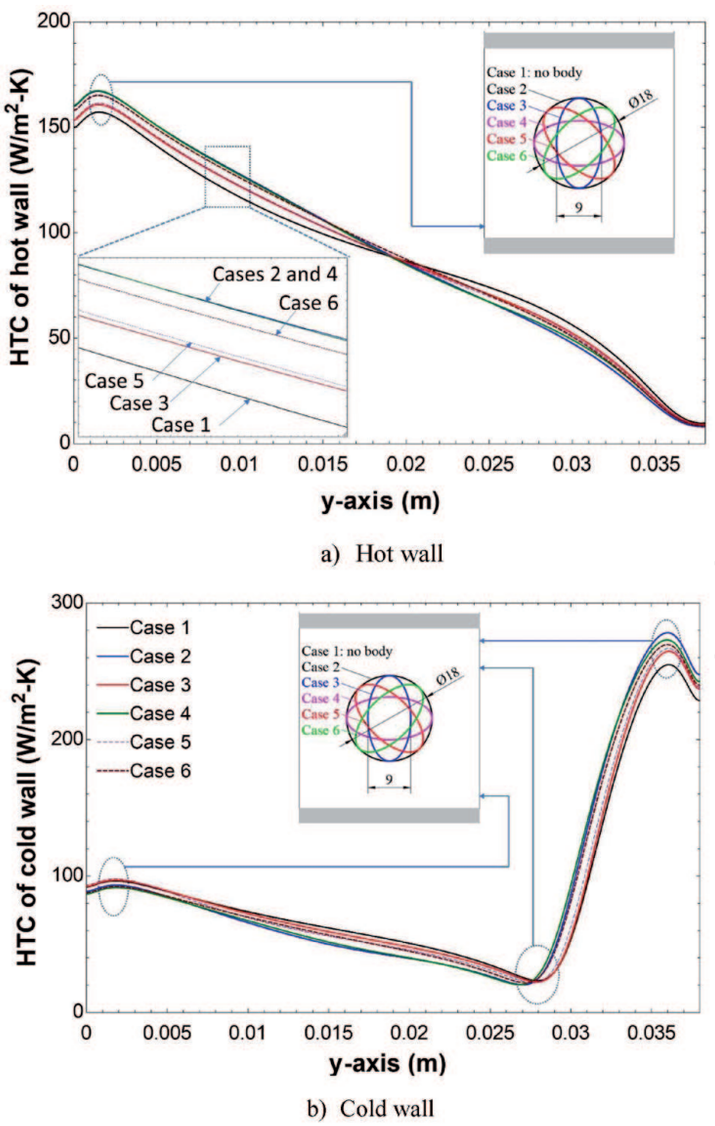

Figure 11.
Local heat transfer coefficient. (a) Hot wall; (b) cold wall.

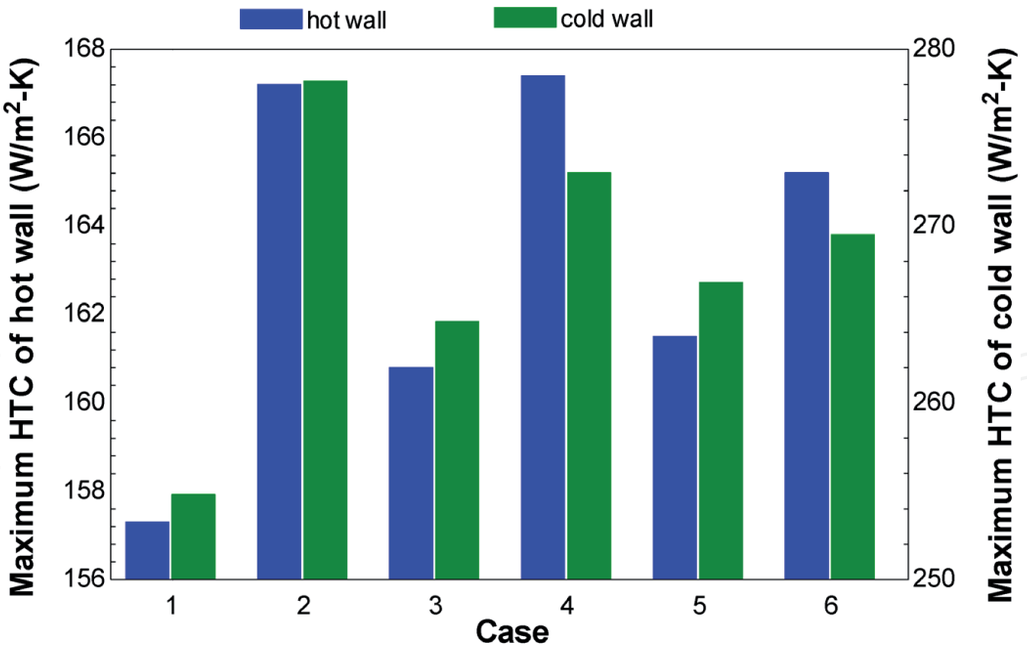

Figure 12.
Comparison of maximum heat transfer coefficient.

with increase in height. This is due to the fact that the fluid increases the temperature leading to reduce the temperature difference between the hot wall and the adjacent fluid. At the top of the hot surface (y = L) the fluid was not moving. Therefore, the convection heat transfer coefficient approaches zero. Body insertion increased the HTC at the best heat transfer position (y ≈ 0). This is because the flow is guided by the body and acts perpendicular to the hot surface as seen in **Figure 5** (point C). In this region, circular body gives the highest heat transfer coefficient because its shape plays a role as a guide vane. Similar phenomena can be observed for HTC of the cold side as shown in **Figure 11b**. At position y = 35 mm HTC is the largest due to impingement heat transfer (see more point D on **Figure 5**). At y = 28 mm (y/L = 0.74), the HTC is approximately zero due to the stagnant fluid as explained above. When y increases from 0 to 28 mm, the HTC decreases due to the decrease in temperature gradient in x-direction. At the best heat transfer position of the cold surface, i.e. y = 35 mm, we can see that the circular body gives the highest HTC and the base case results in the smallest HTC.

Figure 12 compares the maximum heat transfer coefficient on hot (y ≈ 1.5 mm) and cold (y ≈ 35 mm) walls. It can be seen that the HTC of a circle-inserted cavity is 1.06 times (≈ 167/157) higher than that of the base case (Case 1). Once again, we can see that the HTC of cases 2 and 4 is quite identical. Because circular body and elliptical body have the same horizontal dimension (18 mm). The natural convection flow in an enclosure is prevailed by width of a body due to upwelling and downwelling plumes. Among the inserted cavity, case 3 (vertical ellipse) has the smallest HTC due to its smallest horizontal length.

4. Conclusions

The numerical study of the natural convection of water around its maximum density was carried out in this chapter. Fluid-conic structure interaction and natural convection heat transfer were presented and analyzed. The characteristics of temperature distribution, water fluid flow, local entropy generation and local convection heat transfer coefficient were investigated. The main findings from the chapter are as follows:

1. The body insertions prevent the middle downstream causing a slight decrease in fluid velocity.

2. The flow pattern of the circular body and the horizontal elliptical body are nearly identical.

3. The bodies inserted into cavity increase one more primary vortex because of the downward flow separated by bodies.

4. The circular body has the largest entropy generation, the cavity without body yields the smallest entropy generation.

5. Maximum entropy generation occurs at the upper right corner of the cavity. This comes from the huge x-direction temperature variation in this region.

6. Inserts increase the greatest heat transfer coefficient on hot and cold walls. In which the biggest increase is circular body followed by the horizontal elliptical body.

Author details

Nguyen Minh Phu[1,2*] and Nguyen Van Hap[1,2]

1 Faculty of Mechanical Engineering, Ho Chi Minh City University of Technology (HCMUT), Ho Chi Minh City, Viet Nam

2 Vietnam National University, Ho Chi Minh City, Vietnam

*Address all correspondence to: nmphu@hcmut.edu.vn

References

[1] Nguyen MP, Lee G-S. Ice Formation on the Outer Surface of a Vertical Tube with Inside Refrigerant Boiling. Transactions of the Korean Society of Mechanical Engineers B. 2011;**35**(2):129-135 https://doi.org/10.3795/ksme-b.2011.35.2.129

[2] Sasaguchi, K., Kusano, K., Kitagawa, H., & Kuwabara, K. (1997). EFFECT OF DENSITY INVERSION ON COOLING OF WATER AROUND A CYLINDER IN A RECTANGULAR CAVITY. Numerical Heat Transfer, Part A: Applications, 32(2), 131-148. https://doi.org/10.1080/10407789708913884

[3] Sasaguchi, K., Kuwabara, K., Kusano, K., & Kitagawa, H. (1998). Transient cooling of water around a cylinder in a rectangular cavity—a numerical analysis of the effect of the position of the cylinder. International Journal of Heat and Mass Transfer, 41(20), 3149-3156. https://doi.org/10.1016/s0017-9310(98)00064-7

[4] Tong, W. (1999). Aspect ratio effect on natural convection in water near its density maximum temperature. International Journal of Heat and Fluid Flow, 20(6), 624-633. https://doi.org/10.1016/s0142-727x(99)00027-2

[5] Varol, Y., Oztop, H. F., Mobedi, M., & Pop, I. (2010). Visualization of heat flow using Bejan's heatline due to natural convection of water near 4°C in thick walled porous cavity. International Journal of Heat and Mass Transfer, 53(9-10), 1691-1698. https://doi.org/10.1016/j.ijheatmasstransfer.2010.01.020

[6] Hu, Y.-P., Li, Y.-R., & Wu, C.-M. (2014). Comparison investigation on natural convection of cold water near its density maximum in annular enclosures with complex configurations. International Journal of Heat and Mass Transfer, 72, 572-584. https://doi.org/10.1016/j.ijheatmasstransfer.2014.01.047

[7] Cho, H. W., Park, Y. G., & Ha, M. Y. (2018). The natural convection in a square enclosure with two hot inner cylinders, Part I: The effect of one elliptical cylinder with various aspect ratios in a vertical array. International Journal of Heat and Mass Transfer, 125, 815-827. https://doi.org/10.1016/j.ijheatmasstransfer.2018.04.141

[8] Phu, N. M., Bao, T. T., Hung, H. N., Tu, N. T., & Van Hap, N. (2020). Analytical predictions of exergoeconomic performance of a solar air heater with surface roughness of metal waste. Journal of Thermal Analysis and Calorimetry. https://doi.org/10.1007/s10973-020-09787-5

[9] Phu, N. M. (2019). Overall Optimization and Exergy Analysis of an Air Conditioning System Using a Series-Series Counterflow Arrangement of Water Chillers. International Journal of Air-Conditioning and Refrigeration, 27(04), 1950034. https://doi.org/10.1142/s2010132519500342

[10] Nguyen, P. M. (2016). Energy and exergy estimation for a combined cycle of solid CO2 production and NH3-H2O single effect absorption chiller. Science and Technology Development Journal, 19(1), 61-69. https://doi.org/10.32508/stdj.v19i1.611

[11] Luan, N. T., & Phu, N. M. (2020). Thermohydraulic correlations and exergy analysis of a solar air heater duct with inclined baffles. Case Studies in Thermal Engineering, 21, 100672. https://doi.org/10.1016/j.csite.2020.100672

[12] Kashani, S., Ranjbar, A. A., Mastiani, M., & Mirzaei, H. (2014). Entropy generation and natural convection of nanoparticle-water mixture (nanofluid)

near water density inversion in an enclosure with various patterns of vertical wavy walls. Applied Mathematics and Computation, 226, 180-193. https://doi.org/10.1016/j.amc.2013.10.054

[13] Tayebi, T., & Chamkha, A. J. (2019). Entropy generation analysis due to MHD natural convection flow in a cavity occupied with hybrid nanofluid and equipped with a conducting hollow cylinder. Journal of Thermal Analysis and Calorimetry, 139(3), 2165-2179. https://doi.org/10.1007/s10973-019-08651-5

[14] Li, Z., Hussein, A. K., Younis, O., Afrand, M., & Feng, S. (2020). Natural convection and entropy generation of a nanofluid around a circular baffle inside an inclined square cavity under thermal radiation and magnetic field effects. International Communications in Heat and Mass Transfer, 116, 104650. https://doi.org/10.1016/j.icheatmasstransfer.2020.104650

[15] Dalal, A., & Das, M. K. (2005). Laminar natural convection in an inclined complicated cavity with spatially variable wall temperature. International Journal of Heat and Mass Transfer, 48(14), 2986-3007. https://doi.org/10.1016/j.ijheatmasstransfer.2004.07.050

[16] Rhie, C. M., & Chow, W. L. (1983). Numerical study of the turbulent flow past an airfoil with trailing edge separation. AIAA Journal, 21(11), 1525-1532. https://doi.org/10.2514/3.8284

[17] Versteeg, H. K., & Malalasekera, W. (2007). An Introduction to Computational Fluid Dynamics - The finite volume method, Second Edition, Pearson.

[18] Jiannan Tan (2010). A study of solving Navier-Stokes equations with a finite volume method based on polygonal unstructured grids and the computational analysis of ground vehicle aerodynamics, PhD. Dissertation, Texas Tech University.

[19] Michalek, T., Kowalewski, T. A., & Sarler, B. (2005). Natural convection for anomalous density variation of water: numerical benchmark. Progress in Computational Fluid Dynamics, An International Journal, 5(3/4/5), 158. https://doi.org/10.1504/pcfd.2005.006751

[20] Phu, N. M., & Van Hap, N. (2020). Performance Evaluation of a Solar Air Heater Roughened with Conic-Curve Profile Ribs Based on Efficiencies and Entropy Generation. Arabian Journal for Science and Engineering. https://doi.org/10.1007/s13369-020-04676-3

[21] Phu, N. M., & Luan, N. T. (2020). A Review of Energy and Exergy Analyses of a Roughened Solar Air Heater. Journal of Advanced Research in Fluid Mechanics and Thermal Sciences, 77, 160-175.https://doi.org/10.37934/arfmts.77.2.160175